

# Discovering conservation laws from trajectories via machine learning

Seungwoong Ha and Hawoong Jeong\*

Department of Physics, Korea Advanced Institute of Science and Technology, Daejeon 34141, Korea

(Dated: December 23, 2024)

Invariants and conservation laws convey critical information about the underlying dynamics of a system, yet it is generally infeasible to find them without any prior knowledge. We propose ConservNet to achieve this goal, a neural network that extracts a conserved quantity from grouped data where the members of each group share invariants. As a neural network trained with a novel and intuitive loss function called noise-variance loss, ConservNet learns the hidden invariants in each group of multi-dimensional observables in a data-driven, end-to-end manner. We demonstrate the capability of our model with simulated systems having invariants as well as a real-world double pendulum trajectory. ConservNet successfully discovers underlying invariants from the systems from a small number of data points, namely less than several thousand. Since the model is robust to noise and data conditions compared to baseline, our approach is directly applicable to experimental data for discovering hidden conservation laws and relationships between variables.

## I. INTRODUCTION

Modern science greatly depends on the mathematical modeling of given systems and finding the internal structures between observables. One of the most important concepts in system modeling is the *invariants* that underlie the system dynamics, which provide significant information about structural symmetries and low-dimensional embeddings of the system. Invariants and symmetries are fundamental building blocks of nearly all physical systems in nature, such as classical systems with Hamiltonians, Gauge orbits, trajectories under Lorentz transformation, and many dynamical systems with coupled differential equations. Scientists have long attempted to identify the hidden correlations and interactions among the state variables of such systems by discovering the conserved quantities and underlying symmetries.

Recently, under phenomenal advances in machine learning in physical sciences [1–11], various studies have contributed towards the *automation of science* [12–21], referring to current efforts to reveal scientific concepts and construct models solely from observed data without human intervention. Following this line, several studies have attempted to accomplish the automated discovery of conserved quantities with neural networks [18–21]; limitations of these works though include the requirements for additional non-automated preprocessing and often a great number of datasets from different conditions, as well as the ability to only infer the number of invariants. Real-world empirical data are often sparse, noisy, and scattered into small groups, and hence a model for automated discovery needs to be robust to such harsh conditions.

In this study, we introduce ConservNet, a neural network to discover conserved quantities in grouped data, such as trajectories, without any prior knowledge of the

system. Instead of explicitly restricting the model to ensure certain symmetries, we propose a novel loss function that facilitates the model to learn the boundary of the manifold shaped by conservation laws. We show that ConservNet robustly finds a conserved quantity by reducing the intra-group variance of its output while preventing convergence into trivial constant functions. Our model can be applied to a variety of realistic data conditions, is robust to noises and nuisance variables, and employs a pipeline from raw data to invariants in an end-to-end manner that enables the direct extraction of symbolic formulas. We examine the capability of ConservNet to discover conserved quantities by applying it to five model systems ranging from synthetic invariants to physical models that cover diverse functional forms, along with experimental trajectory data of a double pendulum. The robustness of our method strongly demonstrates the potential of ConservNet to be applied to real systems where data is sparse and no conservation laws are known.

## II. METHODS AND MATERIALS

### A. Noise-Variance Loss

Throughout this paper, the data condition  $(N, M)$  indicates that the data is divided into  $N$  groups, in which each group shares the same invariant and has  $M$  data points. Our goal is to find conserved quantities hidden in such grouped  $d$ -dimensional data that are expected to have at least one invariant. In this study, we assume that the system has an invariant function  $V$  that satisfies  $V(x_{ij}) = C_i$  for all  $x_{ij} \in G_i$ , where  $G_i$  denotes the  $i$ -th group. Also, we presume that  $V$  is *meaningful*, implying that the invariant function should show its invariance only for the data with the corresponding symmetry. More formally, let us consider a set of manifolds  $\mathcal{S} = \{\mathcal{M}_1, \mathcal{M}_2, \dots\}$  in which each manifold  $\mathcal{M}_i$  is constructed by removing a degree of freedom as a form of a conservation law with value  $C_i$  from the full space

---

\* Also at Center for Complex Systems, Korea Advanced Institute of Science and Technology, Daejeon 34141, Korea; hjeong@kaist.edu

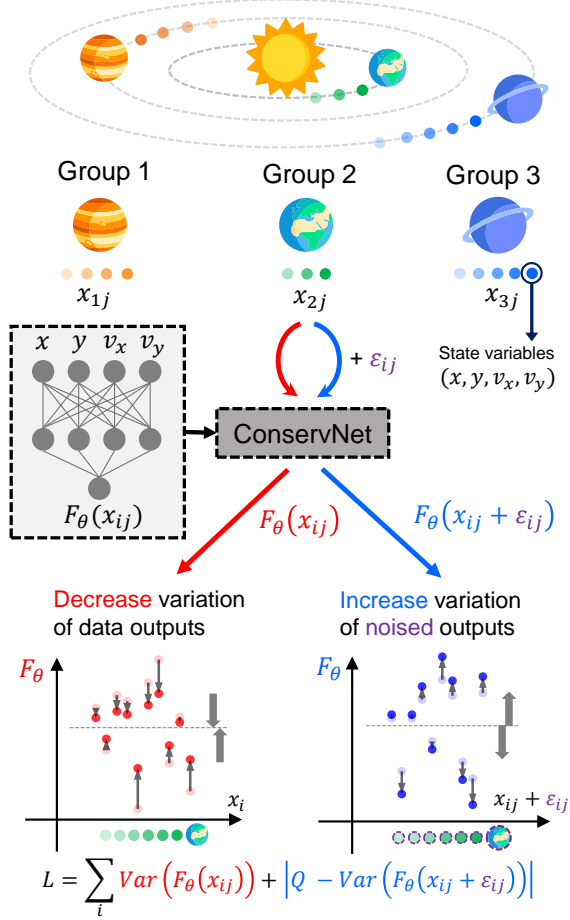


FIG. 1. Overview of ConservNet and schematic description of the role of noise-variance loss. Each group of data  $x_{ij}$ , which is a time series of planet trajectories in this example, is fed into model  $F_\theta$  and optimized to minimize the variance loss  $\text{Var}(F_\theta(x_{ij}))$  and spreading loss  $|Q - \text{Var}(F_\theta(x_{ij} + \varepsilon_{ij}))|$ , with spreading constant  $Q$  and spreading noise  $\varepsilon_{ij}$  restrained by  $R = \max(\|\varepsilon_{ij}\|_2)$ .

$\mathbb{R}^d$ . We presume that our invariant function satisfies  $V(x_{ij}) = C_i$  if and only if  $x_{ij} \in M_i$ .

In order for the model to properly approximate the invariant, it needs to satisfy two important criteria. First, the desired model should produce a ground-truth conserved quantity  $C$ , or at least a value strongly correlated with the true invariant. Second, the model output from the same group should be equal in the ideal case, or at least its deviation should be minimized.

To satisfy the second criteria, the loss function  $L$  for the neural output  $F_\theta$  should decrease the intra-group variance of the outputs from each group, and thus the following variance term should be minimized

$$\mathcal{L}_{i,\text{var}} = \text{Var}(F_\theta(x_{ij})) \quad (1)$$

$$= \left( \frac{1}{M} \sum_j F_\theta(x_{ij})^2 \right) - \left( \frac{1}{M} \sum_j F_\theta(x_{ij}) \right)^2, \quad (2)$$

where  $x_{ij} \in \mathbb{R}^d$  is the  $j$ -th input data of dimension  $d$  from group  $i$ .

Here, the naive optimization of this loss function will generally fall into a trivial minima. As an example, the whole class of simple multivariate function  $f: \mathbb{R}^d \rightarrow C_0$  for any real value  $C_0$  becomes one of the global minima of Eq. 2 since any input will yield a constant and variance becomes zero. Convergence to such a trivial solution would violate the first criteria in our case.

Thus, we have to prevent  $F_\theta$  from trivial convergence to capture a meaningful invariant, which we desire to be a true invariant. One way to inhibit this is by adopting a *spreading* term that increases the variance of the output from improper input, such as input with noise. In this work, we call such outputs from noisy inputs as noised outputs. The key insight here is that since a constant function would yield constant values for every input, we induce the model to not yield constant values from any input data that is *perturbed* from the proper manifold  $M \subset \mathbb{R}^d$ . This spreading loss can be expressed as

$$\mathcal{L}_{i,\text{noise}} = \text{Var}(F_\theta(x_{ij})) + |Q - \text{Var}(F_\theta(x_{ij} + \varepsilon_{ij}))|, \quad (3)$$

where  $Q$  is the spreading constant and  $\varepsilon_{ij}$  denotes a Gaussian noise vector, the  $L_2$  norm of which is bounded to  $R = \max(\|\varepsilon_{ij}\|_2)$ . Here,  $Q$  restricts the absolute value of the variance of the noised output, since optimization without this constraint will lead  $F_\theta$  into a diverging function, ignoring the variance minimization term. Thus, the relative scale of  $Q$  and  $R$  controls the fineness of the spreading. Combining the two terms and summing over all groups, the loss function for ConservNet becomes

$$\mathcal{L} = \sum_i \mathcal{L}_i = \sum_i \text{Var}(F_\theta(x_{ij})) + |Q - \text{Var}(F_\theta(x_{ij} + \varepsilon_{ij}))|. \quad (4)$$

We propose this new loss function for capturing a conserved quantity as noise-variance (NV) loss, as schematically depicted in Fig. 1. One can regard NV loss as a competition between two pressures: one that reduces the variance of the outputs from the given data, and another that increases the variance of the noised output. This balance therefore promotes the neural network to accurately separate the boundary of the manifold from nearby points. ConservNet attempts to find a function that reduces intra-group variance while not being a trivial constant function. We prove that NV loss inhibits trivial convergence by implicitly preventing the divergence of  $F_\theta$  from becoming zero in Appendix A.

TABLE I. Systems and invariants for verification. We use  $\alpha, \beta, \delta, \gamma = (1.1, 0.4, 0.1, 0.4)$  for the Lotka–Volterra system and  $m = 1, GM = 1$  for the Kepler problem. For the double pendulum case, the Hamiltonian of the ideal model is given.

System	Invariant formula
S1	$C = x_1 - 2x_2x_3 + 3x_4^2$
S2	$C = 3x_1 + 2\sin(x_2) + \sqrt{ x_1 x_3^3}$
S3	$C = 2x_1x_2 - (\ln( x_1 + x_3 ) - x_4)/x_3$
Lotka–Volterra	$C = \alpha \ln(x) + \delta \ln(y) - \beta x - \gamma y$
Kepler problem	$C_1 = xv_y - yv_x$
	$C_2 = \frac{1}{2}m(v_x^2 + v_y^2) - \frac{GMm}{r}$
	$C_3 = \mathbf{p} \times \mathbf{L} - mkr\hat{\mathbf{r}}$
Double pendulum (experiment)	$C_{\text{ideal}} = L_1^2(m_1 + m_2)\omega^2 + m_2L_2^2\omega^2$ $+ 2m_1m_2L_1L_2\omega_1\omega_2 \cos(\theta_1 - \theta_2)$
	$-2gL_1(m_1 + m_2) \cos(\theta_1) - 2gm_2L_2 \cos(\theta_2)$

## B. Neural model construction and training

ConservNet is a feed-forward neural network constructed with 4 hidden layers with a layer width of 320 neurons and a single output neuron, using Mish [22] as a non-linear activation function. Our model receives target system data  $x_{ij}$  and produces a single scalar value  $F_\theta(x_{ij})$  that aims to approximate the mapping function from states on the manifolds to conserved quantities. The noise vector  $\varepsilon_{ij}$  is newly sampled from Gaussian distribution at every mini-batch. In practice, we employ standard deviation  $\sigma(x)$  instead of variance  $\text{Var}(x) = \sigma^2(x)$ , and thus Eq. 4 becomes

$$\mathcal{L} = \sum_i \mathcal{L}_i = \sum_i \sigma(F_\theta(x_{ij}) + |Q - \sigma(F_\theta(x_{ij} + \varepsilon_{ij}))|). \quad (5)$$

As a baseline for comparison, we trained a recently proposed Siamese neural network (SNN) [20] along with our model. This SNN architecture extracts an invariant by classifying whether two data points are from the same instance or not, similar to [18]. Both ConservNet and the SNN are trained with Adam [23] optimizer using PyTorch [24] for 50,000 epochs with early stoppings. For all experiments,  $Q = 1$  and spreading noise vector  $\varepsilon_{ij}$  is sampled from the uniform random vector with the maximum norm  $R = 1$  (see Appendix F for details on hyperparameter selection).

## C. Model systems and datasets

In this study, the ability of ConservNet is tested with three synthetic systems, two simulated model systems, and a real double pendulum dataset from [13]. The functional form of each invariant is presented in Table I. Three synthetic systems  $S1$ ,  $S2$ , and  $S3$  are constructed

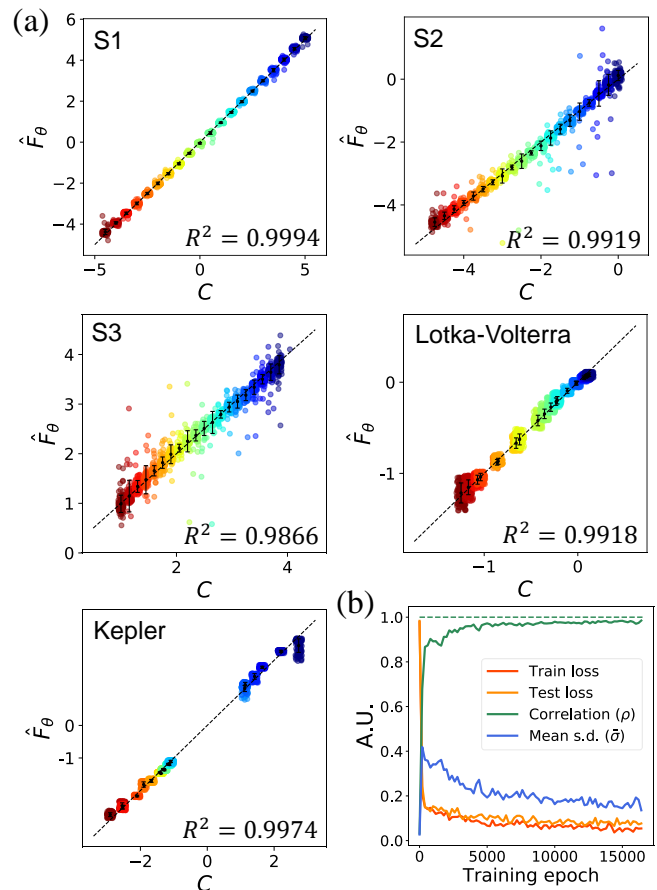


FIG. 2. Model performances of ConservNet. (a) Ground-truth invariants  $C$  versus fitted ConservNet outputs  $\hat{F}_\theta = aF_\theta + b$  for  $S1$ ,  $S2$ ,  $S3$ , the Lotka–Volterra equation, and the Kepler problem are plotted under data condition (20, 100) with  $R^2$  values. Points with the same color share the same invariant values but are plotted at jittered values for visualization. The black dots in each group indicate the invariant and mean output value of that group, with an identity line (black, dotted) drawn for comparison. Error bars denote the standard deviation of each group of data points. For each of the five model systems,  $(a, b)$  is  $(0.31, -0.08)$ ,  $(-0.38, 0.04)$ ,  $(0.21, 0.69)$ ,  $(0.45, 0.01)$ , and  $(0.29, 0.1)$ , respectively. (b) Training loss, test loss, correlation with the ground-truth invariant ( $\rho$ ), and mean intra-group standard deviation ( $\bar{\sigma}$ ) while training 16,000 epochs of ConservNet for invariant  $S2(20, 100)$ . The green dashed line indicates the ideal correlation value 1.

to show a variety of functional forms such as cubic, trigonometric, logarithmic, and rational functions. For the Lotka–Volterra system ( $\frac{dx}{dt} = \alpha x - \gamma xy$ ,  $\frac{dy}{dt} = -\beta y + \delta xy$ ) [25] and the Kepler problem ( $H_{\text{Kepler}} = \frac{\mathbf{p}^2}{2m} - \frac{GMm}{r}$ ), data are simulated by numerical integration with Euler’s method. We find that normalizing the data to match the scale between variables improves overall performances, and thus variables with maximum values exceeding 10 are rescaled by a factor of 0.1. Rescaling inputs also encourages the model output to be more linear with the

true invariant; although unsupervised neural models can learn an arbitrary function of invariant  $h(C(x))$ , the output can still be linearized as  $h(C(x)) = aC(x) + b$  with constants  $a$  and  $b$  if the output range is restricted to a small region.

### III. RESULTS

We prepare 2,000 training data with various data conditions ( $N, M$ ) and an equal number of test data for all simulated systems, which is notable as a small amount compared to modern deep learning and other related studies [19–21] that typically employ more than 10,000 data. These conditions are addressed to replicate practical situations with high data costs and a limited number of different observations, common in physical and biological data. In the case of the real double pendulum data, we use a single trial trajectory with 818 points and divide it into training and test data with a ratio of 8 : 2. The code for dataset generation and model training is publicly available at [26]. For more details about dataset construction and model training, see Appendix B and C.

#### A. Model performances

The model performance of ConservNet is evaluated by the aforementioned two criteria: high correlation with the ground-truth invariant and small intra-group variance. We use Pearson correlation  $\rho$  and mean intra-group standard deviation  $\bar{\sigma} = \frac{1}{N} \sum \sigma_i$  for each criterion.

Figure 2(a) illustrates the notable performances of ConservNet, achieving strong Pearson correlation and small intra-group variation in every model system. For the case of multiple invariants in the Kepler problem, ConservNet captures the angular momentum first and finds the energy secondly when the angular momentum is controlled (see Appendix E for analysis on multiple invariants). Figure 2(b) shows training statistics of ConservNet for  $S2(20, 100)$  as an example case. We can observe that our model shows smooth convergence without overfitting, while its  $\bar{\sigma}$  decreases and  $\rho$  approaches to 1. ConservNet shows consistent performance for different data conditions ( $N, M$ ) as presented in Appendix F.

#### B. Model robustness

We further investigate the capability and robustness of ConservNet by applying several different conditions prevalent in experimental data, and then compare the performance with the baseline SNN. First, we check the impact of noise on the datasets by adding Gaussian noise  $\mathcal{N}(0, s)$  with various strengths  $s$ . Figure 3(a) shows that ConservNet gives consistent performances under the noised condition, with better correlation compared to the baseline. We find that if the data consists of pure noise

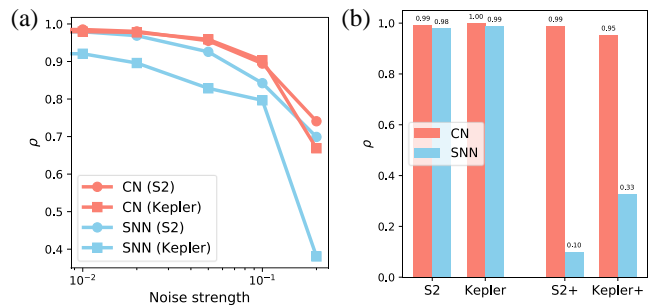


FIG. 3. Robustness of ConservNet (CN). (a) Pearson correlation of ConservNet and SNN for invariant  $S2$  with various noise strengths. (b) Pearson correlation of ConservNet and SNN for two original datasets ( $S2$  and Kepler) and their reinforced versions ( $S2+$  and Kepler+) that include nuisance variables not appearing in the invariants.

without any invariants, our model alerts it by a strong overfitting with high test loss and intra-group variance, as presented in Appendix F.

In a real scenario, there might be irrelevant variables in an observed dataset that do not compose the meaningful invariant. Filtering out such nuisance variables is crucial for data-driven discovery without any prior knowledge. We test our model with two reinforced datasets. First, we concatenate one extra variable  $x_4 \sim \mathcal{N}(0, 1)$  to the  $S2$  dataset to construct  $S2+$  with a noisy variable. Second, we transform the data of the Kepler problem from Cartesian coordinates  $(x, \dot{x}, y, \dot{y})$  into polar coordinates  $(r, \dot{r}, \theta, \dot{\theta})$  to construct Kepler+. In the polar coordinates,  $\theta$  becomes a cyclic coordinate and neither  $\dot{r}$  nor  $\theta$  appears in angular momentum  $r\dot{\theta}$ , different from the original Cartesian form  $x\dot{y} - y\dot{x}$  where all of the state variables appear. The Pearson correlation of each case is plotted in Fig. 4(b), where ConservNet shows robust performances even with the existence of the nuisance variables and coordinate transformation. We find that the SNN strongly overfits and shows low performance when there are unused variables, possibly due to the nature of classifiers and the absence of a proper regularizer.

#### C. Single trajectory of real data

Finally, we apply our model to a real double pendulum trajectory from [13], which is a challenging task in a number of ways. According to [13], the data is extracted from raw video via a motion tracking system, and hence it does not *strictly* obey any conservation laws due to noise and friction. This means that even a perfectly trained model output will not be the same as the ideal Hamiltonian of a double pendulum. Furthermore, the model has to discover the invariant in an extreme data condition where only a single trajectory ( $N = 1$ ) with a limited number of data points ( $M = 654$ ) is available for training. Note that the SNN is inapplicable to this case since it needs

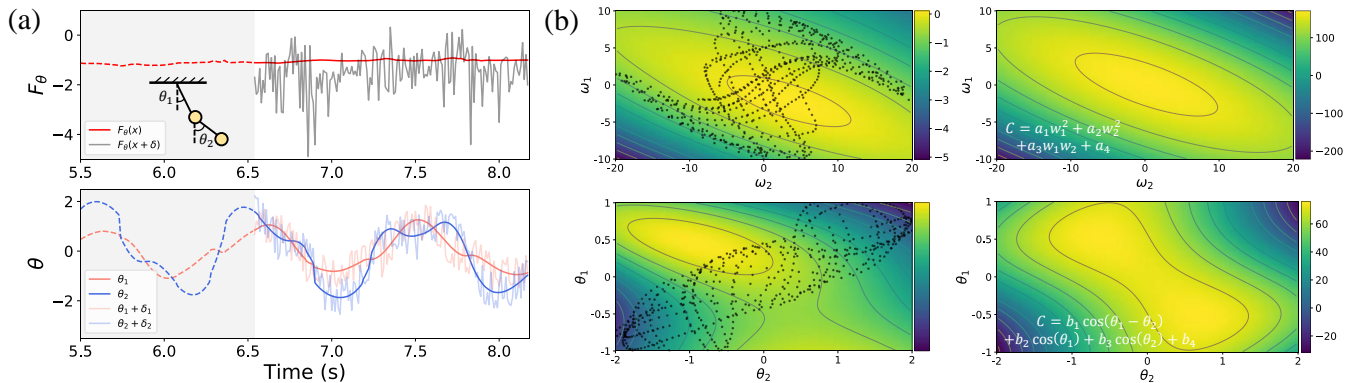


FIG. 4. ConservNet results for real double pendulum data. (a) Model output  $F_\theta(x)$  and the noised model output  $F_\theta(x + \varepsilon)$  with  $\varepsilon = (\varepsilon_1, \varepsilon_2)$  (top), and double pendulum trajectories  $\theta_1, \theta_2$  and noised trajectories (bottom) versus time. Data in the shaded area are used for training (from 0 s to 6.54 s), with the remaining data used for testing (6.54 s to 8.18 s). (b) 2D heatmap of model output  $F_\theta$  (left) and ideal Hamiltonian (right) for  $(\theta_1, \theta_2, \omega_1, \omega_2) = (0, 0, \omega_1, \omega_2)$  (top) and  $(\theta_1, \theta_2, \omega_1, \omega_2) = (\theta_1, \theta_2, 5, 10)$  (bottom). The training data points are scattered in the left panels, while the ideal formulas for the cross-section are presented in the right panels. Here, the ideal heatmaps are drawn with constants  $(a_1, a_2, a_3, a_4 = 1, 0.32, 0.82, -170.95)$  and  $(b_1, b_2, b_3, b_4 = 41, -124.13, -46, 82, 57)$ , provided by [13].

at least two groups of data to compare ( $N \geq 2$ ).

We train our model and examine its output for stability and accuracy. Figure 4a shows that ConservNet output  $F_\theta$  stably remains constant for the training and test trajectory but not for the noised trajectory, verifying that ConservNet falls into neither trivial convergence nor overfitting and properly captures the functional form of the invariant. We further check two-dimensional cross-sections of the model output by fixing two variables and varying two variables, and compare them with the cross-sections of the ideal four-dimensional Hamiltonian, constructed with the constants from [13]. The results are shown in Fig. 4b. Considering inherent frictions and the restricted regions of the data points, both heatmaps are similar enough to the point where the inference of the abstract functional form is possible, especially at the regions where the data points present. To summarize, ConservNet successfully captured the conserved quantity from a real double pendulum system with extreme data conditions.

#### IV. DISCUSSION

We have introduced ConservNet, a neural framework to discover a conserved quantity from grouped data. Interpreting the results of the model output shows that ConservNet learns meaningful invariants in the systems with various data conditions, even a single trajectory. In real practice where the ground-truth invariant is unknown, we may identify the symbolic form of the invariant by sorting the output values and employing off-the-shelf polynomial regression or symbolic regression algorithms. We illustrate a result of such application for invariant S1 as an example in Appendix D, in which the ground-truth symbolic formula was successfully re-

trieved. In cases with an insufficient number of groups to perform such regression, one can attempt to infer the functional form by examining its output and cross-sections, as we have done for the real double pendulum data.

One limitation that ConservNet shares with [20] is that the single model finds a single invariant even if the system could have multiple invariants. While we showed that training with modified data leads to the discovery of remaining invariants, such modification is usually impossible for experimental data and the total number of conserved quantities remains unknown in general. Since our model identifies the numerical value of the conserved quantity and [21] approximates the number of conserved quantities, unifying the advantages of these approaches would be an interesting future direction to be explored.

#### ACKNOWLEDGMENTS

This research was supported by the Basic Science Research Program through the National Research Foundation of Korea NRF-2017R1A2B3006930.

#### Appendix A: Proof for Noise-Variance Loss

##### 1. Simple loss and its limitation

In this study, we assume that the dataset consists of  $N$  groups with group size  $M$ , and has a meaningful invariant function  $V$  that satisfies  $V(x_{ij}) = C_i$  for all  $x_{ij} \in G_i$ , where  $G_i$  denotes the  $i$ -th group.

One may construct a simple loss function with a variance-decreasing term only, such as

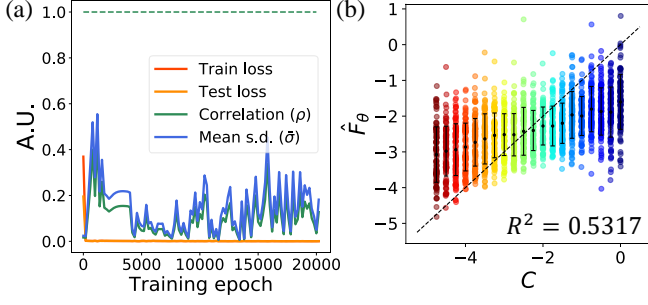


FIG. 5. Model performances of ConservNet where the model is trained with  $\mathcal{L}_{\text{simple}}$ . (a) Training loss, test loss, correlation with ground-truth invariant ( $\rho$ ), and mean intra-group standard deviation ( $\bar{\sigma}$ ) during training 20,000 epochs for invariant  $S2(20, 100)$ . The green dashed line indicates the ideal correlation value 1. (b) Ground-truth invariants  $C$  versus fitted ConservNet outputs  $\hat{F}_\theta = aF_\theta + b$  for the invariant  $S2$  plotted under data condition  $(20, 100)$  with the  $R^2$  value. Here,  $(a, b) = (8.88 \times 10^{-5}, 0.92 \times 10^{-4})$ .

$$\mathcal{L}_{\text{simple}} = \sum_i \mathcal{L}_{\text{simple},i} = \sum_i \text{Var}(F_\theta(x_{ij})), \quad (\text{A1})$$

where  $x_{ij}$  is an input data. It is simple to show that by performing gradient descent on  $\mathcal{L}_{\text{simple}}$  for the network parameters  $\theta$ , the output from the same group will approach the same constant value.

**Theorem A.1.** *The global minimum of the functional  $\mathcal{L}_{\text{simple}}$  is  $F_\theta(x_{ij}) = C_i$  with some constant  $C_i$  for all groups.*

*Proof of Theorem A.1.* Neural model  $F_\theta$  tunes the output by optimizing  $F_{\theta,ij} = F_\theta(x_{ij})$  through the network parameter  $\theta$ . The condition of  $\mathcal{L}_{\text{simple},i}$  for the stationary point becomes

$$\frac{\partial \mathcal{L}_{\text{simple},i}}{\partial F_{\theta,ij}} = \frac{\partial}{\partial F_{\theta,ij}} \text{Var}(F_{\theta,ij}) = 0 \quad (\text{A2})$$

for all  $F_{\theta,ij}$ . By expanding the variance function with  $\mu_i^F = \frac{1}{M} \sum_j F_{\theta,ij}$ , we get

$$\begin{aligned} & \frac{\partial \mathcal{L}_{\text{simple},i}}{\partial F_{\theta,ij}} \quad (\text{A3}) \\ &= \frac{1}{M} \frac{\partial}{\partial F_{\theta,ij}} \sum_j (F_{\theta,ij} - \mu_i^F)^2 \\ &= \frac{1}{M} \sum_j 2(F_{\theta,ij} - \mu_i^F) \frac{\partial F_{\theta,ij} - \mu_i^F}{\partial F_{\theta,ij}} \\ &= \frac{2}{M} (F_{\theta,ij} - \mu_i^F) - \frac{2}{M^2} \sum_j (F_{\theta,ij} - \mu_i^F) \\ &= \frac{2}{M} (F_{\theta,ij} - \mu_i^F) = 0, \end{aligned}$$

since  $\sum_j (F_{\theta,ij} - \mu_i^F) = 0$ . This means  $F_{\theta,ij} = \mu_i^F$  at the stationary point, indicating that every  $F_{\theta,ij}$  is a constant  $C_i = \mu_i^F$ . Also, by checking its second derivative, we get

$$\begin{aligned} \frac{\partial^2 \mathcal{L}_{\text{simple},i}}{\partial F_{\theta,ij}^2} &= \frac{\partial}{\partial F_{\theta,ij}} \frac{2}{M} (F_{\theta,ij} - \mu_i^F) \quad (\text{A4}) \\ &= \frac{2}{M} \left(1 - \frac{1}{M}\right) > 0 \end{aligned}$$

since  $M$  is a natural number. Hence, this stationary point is the global minimum.

**Corollary A.1.1.** *The constant function  $F_{\text{const}}(x) = C_0$  for any  $x \in \mathbb{R}^d$  satisfies the condition for the global minimum of the functional  $\mathcal{L}_{\text{simple}}$ .*

□

Obviously, the intra-group variance will be 0 if all of the model output from the same group becomes the same constant. But the zero intra-group variance is not a sufficient condition for a meaningful invariant, as mentioned in the main manuscript. Any modern deep learning architecture with perceptrons and feed-forward networks (including ConservNet) can express the constant function by reducing the weight to zero (i.e., ignoring the input completely), and hence is prone to learn such a simple function rather than a meaningful invariant. In Fig. 5, we can see that the model trained with  $\mathcal{L}_{\text{simple}}$  falls into this trap; it does not properly capture the given invariant, and instead shows nearly constant behavior even though the training and test loss rapidly converged to zero in the early stages of training.

## 2. Noise-variance loss

Now, we focus on the proposed noise-variance loss (NV loss) for ConservNet:

$$\mathcal{L} = \sum_i \mathcal{L}_i = \sum_i \underbrace{\text{Var}(F_\theta(x_{ij}))}_{\mathcal{A}_i} + \underbrace{|Q - \text{Var}(F_\theta(x_{ij} + \varepsilon_{ij}))|}_{\mathcal{B}_i}, \quad (\text{A5})$$

where  $Q$  is a spreading constant and  $\varepsilon_{ij}$  denotes a spreading noise vector. The function consists of the same term as  $\mathcal{L}_{\text{simple}}$  ( $\mathcal{A}_i$ ) and an additional term that keeps the variance of the noised output at a certain value ( $\mathcal{B}_i$ ). We want to show that the minimization of this loss function will avoid trivial convergence by flipping its behavior when the noised output variance becomes too low.

**Theorem A.2.** *The constant function  $F_{\text{const}}(x) = C_0$  for all  $x \in \mathbb{R}^d$  and some constant  $C_0$  is not a minima of  $\mathcal{L}_i$ .*

*Proof of Theorem A.2.* To find a stationary point, we again apply a partial derivative to  $\mathcal{L}$ . Due to the absolute value in  $\mathcal{B}_i$ , the partial derivative becomes

$$\begin{aligned} \frac{\partial}{\partial F_{\theta,ij}} |\mathcal{B}_i| &= \frac{\partial}{\partial F_{\theta,ij}} \sqrt{\mathcal{B}_i^2} = \text{sgn}(\mathcal{B}_i) \frac{\partial \mathcal{B}_i}{\partial F_{\theta,ij}} \quad (\text{A6}) \\ &= -\text{sgn}(\mathcal{B}_i) \left[ \frac{\partial}{\partial F_{\theta,ij}} \text{Var}(F_{\theta}(x_{ij} + \varepsilon_{ij})) \right]. \end{aligned}$$

By expanding this expression with Taylor expansion, we get

$$\begin{aligned} -\text{sgn}(\mathcal{B}_i) \left[ \frac{\partial}{\partial F_{\theta,ij}} \text{Var}(F_{\theta}(x_{ij} + \varepsilon_{ij})) \right] &= -\text{sgn}(\mathcal{B}_i) \left[ \frac{\partial}{\partial F_{\theta,ij}} \text{Var}(F_{\theta,ij} + \nabla F_{\theta,ij} \varepsilon_{ij} + \mathcal{O}(\varepsilon_{ij}^2)) \right] \quad (\text{A7}) \\ &= -\text{sgn}(\mathcal{B}_i) \left[ \frac{1}{M} \frac{\partial}{\partial F_{\theta,ij}} \sum_j (F_{\theta,ij} + \nabla F_{\theta,ij} \varepsilon_{ij} - \mu_i^{F\nabla})^2 \right] \\ &= -\text{sgn}(\mathcal{B}_i) \left[ \frac{1}{M} \sum_j 2(F_{\theta,ij} + \nabla F_{\theta,ij} \varepsilon_{ij} - \mu_i^{F\nabla}) \frac{\partial (F_{\theta,ij} + \nabla F_{\theta,ij} \varepsilon_{ij} - \mu_i^{F\nabla})}{\partial F_{\theta,ij}} \right] \\ &= -\text{sgn}(\mathcal{B}_i) \left[ \frac{2}{M} (F_{\theta,ij} + \nabla F_{\theta,ij} \varepsilon_{ij} - \mu_i^{F\nabla}) - \frac{2}{M^2} \sum_j F_{\theta,ij} + \nabla F_{\theta,ij} \varepsilon_{ij} - \mu_i^{F\nabla} \right] \\ &= -\text{sgn}(\mathcal{B}_i) \frac{2}{M} (F_{\theta,ij} + \nabla F_{\theta,ij} \varepsilon_{ij} - \mu_i^{F\nabla}), \end{aligned}$$

where  $\frac{\partial \nabla F_{\theta,ij} \varepsilon_{ij}}{\partial F_{\theta,ij}} = 0$  and  $\mu_i^{F\nabla} = \frac{1}{M} \sum_j F_{\theta,ij} + \nabla F_{\theta,ij} \varepsilon_{ij}$ .  
Combining these two terms,  $\mathcal{A}_i$  and  $\mathcal{B}_i$ , the entire par-

tial derivative has two cases depending on the sign of  $\mathcal{B}_i$ :

$$\begin{aligned} \frac{\partial \mathcal{L}}{\partial F_{\theta,ij}} &= \begin{cases} \frac{2}{M} [(F_{\theta,ij} - \mu_i^F) - (F_{\theta,ij} + \nabla F_{\theta,ij} \varepsilon_{ij} - \mu_i^{F\nabla})] & \text{if } \text{sgn}(\mathcal{B}_i) = 1 \\ \frac{2}{M} [(F_{\theta,ij} - \mu_i^F) + (F_{\theta,ij} + \nabla F_{\theta,ij} \varepsilon_{ij} - \mu_i^{F\nabla})] & \text{if } \text{sgn}(\mathcal{B}_i) = -1 \end{cases} \quad (\text{A8}) \\ &= \begin{cases} \underbrace{\frac{2}{M} [(\mu_i^\nabla - \nabla F_{\theta,ij} \varepsilon_{ij})]}_{\mathcal{C}_i} & \text{if } \text{sgn}(\mathcal{B}_i) = 1 \\ \underbrace{\frac{2}{M} [(2F_{\theta,ij} + \nabla F_{\theta,ij} \varepsilon_{ij} - (\mu_i^{F\nabla} + \mu_i^F))]}_{\mathcal{D}_i} & \text{if } \text{sgn}(\mathcal{B}_i) = -1, \end{cases} \end{aligned}$$

where  $\mu_i^\nabla = \frac{1}{M} \sum_j \nabla F_{\theta,ij} \varepsilon_{ij}$ . When the noised output variance is greater than  $Q$  ( $\mathcal{C}_i$ ), both terms cooperate to reduce the variance of  $F_{\theta}$  regardless of the input. But when the noised output variance becomes smaller than  $Q$ , the terms that contributed to the cooperation cancel out, and the functional now has a global maximum instead of a global minimum. In this regime, the constant function becomes the only solution, as follows.

**Lemma A.3.** *A constant function  $F_{\text{const}}(x) = C_0$  for all  $x \in \mathbb{R}^d$  and some constant  $C_0$  is a global maximum of  $\mathcal{L}_i$  when  $\text{sgn}(\mathcal{B}) = 1$ .*

*Proof of Theorem A.3.* First,  $\mathcal{C}_i$  has its critical point when every  $\nabla F_{\theta,ij} \varepsilon_{ij}$  becomes a constant  $\mu_i^\nabla$ . This is a global maximum since any deviation from the constant will decrease  $(\mu_i^\nabla - \nabla F_{\theta,ij} \varepsilon_{ij})$ , as the second derivative test shows,

$$\begin{aligned} \frac{\partial^2 \mathcal{L}_{i,\text{sgn}(\mathcal{B}_i)=1}}{\partial \nabla F_{\theta,ij} \varepsilon_{ij}^2} &= \frac{\partial}{\partial \nabla F_{\theta,ij} \varepsilon_{ij}} \frac{2}{M} (\mu_i^\nabla - \nabla F_{\theta,ij} \varepsilon_{ij}) \quad (\text{A9}) \\ &= \frac{2}{M} \left( \frac{1}{M} - 1 \right) < 0. \end{aligned}$$

Since the noise vector  $\varepsilon_{ij}$  can have an arbitrary value,

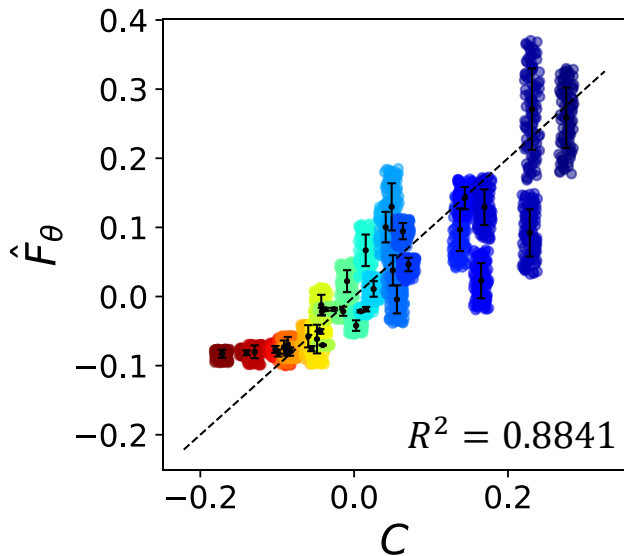


FIG. 6. Ground-truth invariants  $C$ , i.e. the total energy, versus fitted ConservNet outputs  $\hat{F}_\theta = aF_\theta + b$  for the Kepler problem plotted under data condition (20, 100) with the  $R^2$  value, from a controlled dataset where angular momentum over the dataset is fixed to  $L = -1.5$ . Here,  $(a, b) = (-2.61, -0.29)$ .

the only way to satisfy the condition for the global maximum is that  $\nabla F_{\theta,ij} = 0$ , which means that the function is a constant everywhere.  $\square$

Now, suppose that the constant function is one of the minima of  $\mathcal{L}_i$ . Then, it can only exist at the region where  $\text{sgn}(\mathcal{B}_i) = -1$  according to Lemma A.3. But, the constant function always yields  $\text{sgn}(\mathcal{B}_i) = 1$  since  $\mathcal{B}_i = Q - \text{Var}(F_\theta(x_{ij} + \varepsilon_{ij})) = Q - 0 = Q > 0$ . This is contradictory, and hence the constant function cannot be a minimum of the NV loss.  $\square$

Intuitively, NV loss prevents trivial convergence by maintaining a non-zero value for the divergence of  $F_\theta$ , which cannot be accomplished by the constant function.

## Appendix B: Dataset Detail

We prepare total six systems for training:  $S1$ ,  $S2$ ,  $S3$ , the Lotka–Volterra system, the Kepler problem, and observation data from a real double pendulum. Table II shows the exact range and sample distribution of each variable in every model system.

### 1. Synthetic systems

The datasets are composed by first randomly drawing the relative variables except for the final one, and calcu-

lating the last relative variable which preserves the overall conserved quantity. We tried to maximize the variety of simulated data by setting the noise distribution and variable range for each system as differently as possible. While producing each dataset, we restricted the absolute value of the output of the final variable, consequently rejecting some perilous set of variables that forces the last variable into an extremely diverging value.

### 2. Physical systems

We generate the data from physical systems by integrating respective differential equations with Euler’s method and performing subsampling to the trajectories. For the Lotka–Volterra system, we simulate the dynamics for  $100M$  steps for the dataset of batch size  $M$  with time interval  $dt = 0.01$ . The obtained data are further subsampled at every 100 steps, effectively setting the time interval between data points to 1. We scale  $x, y$  in the Lotka–Volterra equation and the position coordinates  $x, y$  in the Kepler problem by a factor of 0.1.

### 3. Real double pendulum

Double pendulum data is adopted from [13], where two trials of double pendulum data are available. We use the first trial, consisting of 818 data points with four-dimensional time-series  $(\theta_1, \theta_2, \omega_1, \omega_2)$ . Each data point corresponds to 0.01 s, making the total data length 8.18 s. The training set consists of the first  $654 = 818 \times 0.8$  points, and the test set consists of the remaining  $154 = 818 \times 0.2$  points. We scale  $\omega_1, \omega_2$  by a factor of 0.1 to match the  $\theta_1$  and  $\theta_2$  scale.

## Appendix C: Training Detail

Both the SNN and ConservNet are composed of six layers of multi-layer perceptrons (MLPs) with a layer width of 320, where the input dimension varies by the target system and has a single output neuron. Note that the original SNN [17] used two layers of MLPs with a layer width of 160; we found that increasing the layer depth and width generally increased the overall performances for both SNN and ConservNet.

During training, we found the training result of SNN significantly varies by random initialization and is highly prone to overfitting. We report that the SNN shows a good performance (training and test accuracy of 100% and 99.75% with correlation 0.998) in one trial but converges to a meaningless output with strong overfitting (training and test accuracy of 100% and 50.03% with correlation 0.154) in the very next trial with the same conditions. In several trials, a larger layer width (320) exhibits strong overfitting while a relatively shallow one (160) shows better generalization performances.

TABLE II. Variable range and sample distribution of training and test data for each system. Variables with a star (\*) in the distribution column are calculated after the other variables were drawn from the sample distribution, while the dash (-) indicates a non-samplable variable. For physical systems (Lotka–Volterra and the Kepler problem), the distribution column indicates each variable’s initial distribution (and hence differs from the actual range as shown). In the remarks column, the term *rescaled* means that the variables are normalized by a given factor before constructing the dataset for the model training.

Invariant	System formula	Variable	Distribution	Actual range	Remarks
S1	$C = x_1 - 3x_2x_3 + \frac{1}{2}x_4^2$	$x_1$	*	[-4.99, 4.99]	Model invariant
		$x_2$	$\sim \mathcal{N}(0, 2)$	[-6.73, 6.90]	
		$x_3$	$\sim \mathcal{N}(0, 2)$	[-6.39, 5.60]	
		$x_4$	$\sim \mathcal{N}(0, 2)$	[-5.41, 5.70]	
		$C$	-	[-4.5, 5.0]	
S2	$C = 3x_1 + 2\sin(x_2) + \sqrt{ x_1 }x_3^3$	$x_1$	$\sim \mathcal{U}(-3, 3)$	[-2.99, 0.52]	Model invariant
		$x_2$	*	[-9.42, 9.42]	
		$x_3$	$\sim \mathcal{U}(-3, 3)$	[-2.89, 2.90]	
		$C$	-	[-5.0, 0.0]	
S3	$C = 2x_1x_2 - (\ln( x_1 + x_3 ) - x_4)/x_3$	$x_1$	*	[-9.94, 9.99]	Model invariant
		$x_2$	$\sim \mathcal{U}(-10, 10)$	[-9.93, 9.98]	
		$x_3$	$\sim \mathcal{U}(0.5, 5)$	[0.50, 4.99]	
		$x_4$	$\sim \mathcal{U}(-10, 10)$	[-9.92, 9.98]	
		$C$	-	[1.0, 3.85]	
Lotka–Volterra	$C = \alpha \ln(x) + \delta \ln(y) - \beta x - \gamma y$	$x_1$	$\sim \mathcal{U}(1, 10)$	[0.004, 25.53]	$x_1, x_2$ rescaled (0.1)
		$x_2$	$\sim \mathcal{U}(1, 10)$	[0.03, 9.77]	
		$C$	-	[-1.24, 0.12]	
Kepler problem	$C_1 = xv_y - yv_x$	$x$	*	[-5, 5]	Eccentricity $e < 0.99$ $x, y$ rescaled (0.1)
		$y$	$\sim \mathcal{U}(-5, 5)$	[-9.74, 15.28]	
		$v_x$	$\sim \mathcal{U}(-5, 5)$	[-1.49, 1.08]	
		$v_y$	$\sim \mathcal{U}(-5, 5)$	[-1.43, 1.39]	
		$C_1$	-	[1.0, 3.85]	
Double pendulum	$C_{\text{ideal}} = L_1^2(m_1 + m_2)\omega^2 + m_2L_2^2\omega^2 + 2m_1m_2L_1L_2\omega_1\omega_2 \cos(\theta_1 - \theta_2) - 2gL_1(m_1 + m_2) \cos(\theta_1) - 2gm_2L_2 \cos(\theta_2)$	$\theta_1$	-	[-1.39, 1.42]	$\omega_1, \omega_2$ rescaled (0.1)
		$\theta_2$	-	[-2.14, 2.15]	
		$\omega_1$	-	[-10.60, 10.46]	
		$\omega_2$	-	[-21.21, 21.37]	

For a fair comparison, we test every combination of learning rates [0.005, 0.0005, 0.00005] and layer widths [160, 320], and report the best performing one (in terms of test accuracy) among five trials for each condition as representative results of the SNN. In the case of ConservNet, we fix the learning rate at 0.00005 and layer width at 320 neurons since the performance was robust against both layer width and learning rate. We train both the SNN and ConservNet for 50,000 epochs with early stopping, Adam[23] optimizer, and no particular regularizer. The batch size for mini-batch training is fixed to 64 for the SNN and tentative for Conservnet, where its batch size is fixed as respective group size  $M$ . Training takes several hours on a single GeForce GTX 1080, depending on the batch size.

#### Appendix D: Extraction of symbolic formula from ConservNet results

In a real scenario, identifying the explicit functional form of the invariant rather than just a numerical value of the invariant is often crucial for understanding the system and its inherent symmetry. This can be done by performing polynomial or symbolic regression on the ConservNet output, as mentioned in the main manuscript, but many regression methods are prone to overfitting if the data is erroneous. Hence, besides its usefulness, the successful retrieval of symbolic functions from data also indicates the high quality of the model output. As an exemplary case, we perform ridge regression with polynomial features of the input data on the output of ConservNet for invariant  $S1$ . The result of the regression for order 2 is

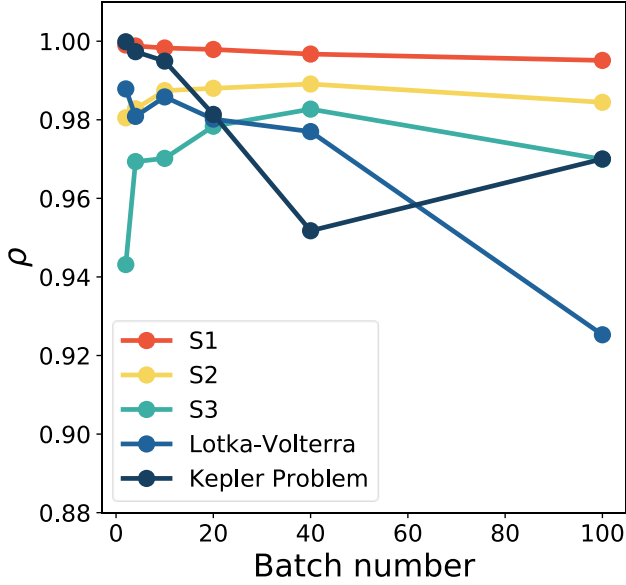


FIG. 7. Pearson correlation  $\rho$  with varying data conditions during 50,000 epochs of training ConservNet for the invariants. Here, the total data number is fixed to 2,000 and hence the data conditions of (2, 1000), (4, 500), (10, 200), (20, 100), (40, 50), and (100, 20) are tested.

$$\begin{aligned}
 F_\theta &= 0.3069x_1 + 0.0005x_2 - 0.0019x_3 + 0.0035x_4 \quad (\text{D1}) \\
 &+ 0.0005x_1^2 + 0.0006x_1x_2 - 0.0006x_1x_3 + 0.0002x_1x_4 \\
 &- 0.0006x_2^2 - 0.921x_2x_3 - 0.0002x_2x_4 + 0.0008x_3^2 \\
 &+ 0.0004x_3x_4 + 0.1528x_4^2 \\
 &\approx 0.3x_1 - 0.9x_2x_3 + 0.15x_4^2.
 \end{aligned}$$

We can see that the approximated output is the same as  $\frac{3}{10}S1$ , showing that ConservNet can provide reliable output for the extraction of symbolic formulas.

#### Appendix E: ConservNet for a system with multiple invariants

In the main manuscript, we show that ConservNet discovers angular momentum in the Kepler problem among three possible invariants. Since the model is designed to output a single value from a single output, jointly finding multiple invariants needs a modification to the current architecture. In [20], the authors verified their model (SNN) by fixing the angular momentum of the given dataset and performing the same training. We test our model with similar settings using a controlled dataset to examine whether the model can discover a second invariant. Figure 6 shows that the model output shows a strong correlation with a second invariant, namely the total energy of the orbital system, from the controlled

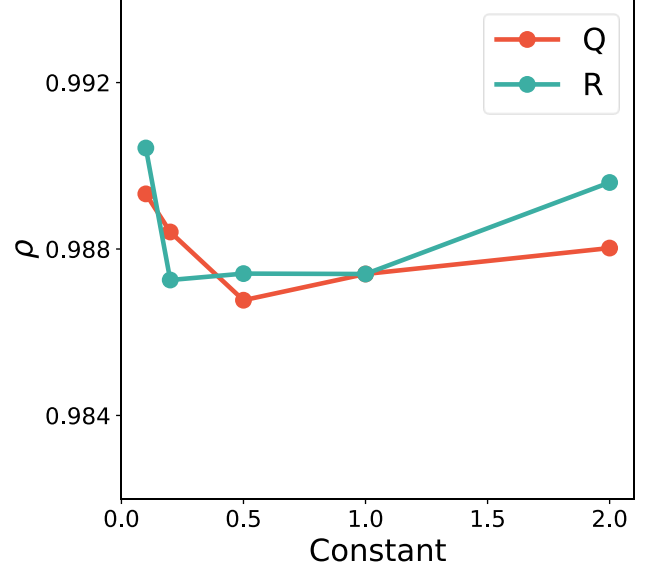


FIG. 8. Pearson correlation  $\rho$  with varying spreading constant  $Q$  (fixed  $R = 1$ ) and max noise norm  $R$  (fixed  $Q = 1$ ) during 20,000 epochs of training ConservNet for the invariant  $S2$ .

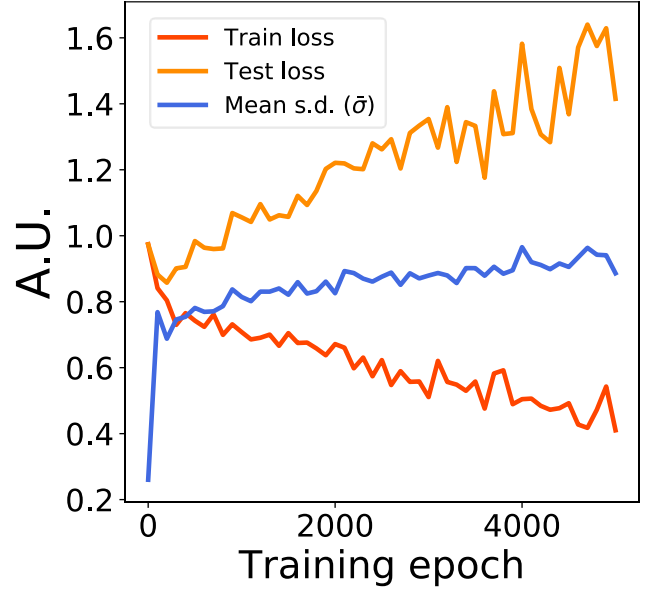


FIG. 9. Training loss, test loss, and mean intra-group standard deviation ( $\bar{\sigma}$ ) during 5,000 epochs of training ConservNet for random data.

dataset. Modifying ConservNet for the simultaneous discovery of multiple invariants would be an interesting future direction.

## Appendix F: Robustness of ConservNet performances in various conditions

### 1. Results with various data conditions

In the main manuscript, we fixed all of the simulated data conditions to  $(20, 100)$ . In this section, we further test different data conditions with different batch numbers and batch sizes while fixing the total number of data points to 2,000. In Fig. 7, the correlation  $\rho$  for all five simulated systems with different data conditions are plotted. We can confirm that ConservNet shows good performances ( $\rho > 0.9$ ) for all simulated settings, including both extreme ends: from the points where only a single, long dataset is possible, to the points where a hundred different trials with a short period of observation was recorded.

### 2. Hyperparameters and spreader selection

In the main manuscript, we set  $Q = 1$  and  $R = 1$  for all experiments. But in our NV loss, the relative magnitude between  $Q$  and  $R$  determines the strength of the spreader, and one may raise a question about the relationship between such a specific choice of hyperparameters and the model performance. To test the robust-

ness of ConservNet with other hyperparameters, we use  $S2(20, 100)$  as a test invariant and record the Pearson correlation  $\rho$  while varying  $Q$  and  $R$  values. The results are shown in Fig. 8, which verify that the model performances are practically unaffected by the choice of specific hyperparameters.

We also test different types of spreaders by restraining the noise with different norms. Instead of  $L_2$ -norm we use in the main experiment, we test  $L_1$ -norm and  $L_\infty$ -norm to be restrained to 1. As a result, both spreaders achieve comparable results of 0.9910 and 0.9862, respectively, for  $S2(20, 100)$ . To sum up, ConservNet is robust to both hyperparameter selection and spreader type, implying that the spreader can be freely constructed as long as it serves the main purpose: preventing the model from trivial convergence.

### 3. System with no specific invariant

If the system under study has no specific invariant, a good model for invariant discovery should notice such an absence. We train ConservNet with random data consisting of five-dimensional Gaussian random vector  $X \sim \mathcal{N}(\mu, \Sigma)$ , where  $\mu \in \mathbb{R}^5$  and  $\Sigma = I_5$ . ConservNet alerts the absence of an invariant by showing strong overfitting and large intra-group deviations, as shown in Fig. 9.

- 
- [1] J. Carrasquilla and R. G. Melko, Machine learning phases of matter, *Nature Physics* **13**, 431 (2017).
  - [2] K. Ch'Ng, J. Carrasquilla, R. G. Melko, and E. Khatami, Machine learning phases of strongly correlated fermions, *Physical Review X* **7**, 031038 (2017).
  - [3] E. P. Van Nieuwenburg, Y.-H. Liu, and S. D. Huber, Learning phase transitions by confusion, *Nature Physics* **13**, 435 (2017).
  - [4] Y. Zhang and E.-A. Kim, Quantum loop topography for machine learning, *Physical Review Letters* **118**, 216401 (2017).
  - [5] G. Carleo and M. Troyer, Solving the quantum many-body problem with artificial neural networks, *Science* **355**, 602 (2017).
  - [6] P. Baldi, P. Sadowski, and D. Whiteson, Searching for exotic particles in high-energy physics with deep learning, *Nature communications* **5**, 1 (2014).
  - [7] P. Ponte and R. G. Melko, Kernel methods for interpretable machine learning of order parameters, *Physical Review B* **96**, 205146 (2017).
  - [8] P. Zhang, H. Shen, and H. Zhai, Machine learning topological invariants with neural networks, *Physical Review Letters* **120**, 066401 (2018).
  - [9] N. Sun, J. Yi, P. Zhang, H. Shen, and H. Zhai, Deep learning topological invariants of band insulators, *Physical Review B* **98**, 085402 (2018).
  - [10] G. Torlai, G. Mazzola, J. Carrasquilla, M. Troyer, R. Melko, and G. Carleo, Neural-network quantum state tomography, *Nature Physics* **14**, 447 (2018).
  - [11] M. Rafayelyan, J. Dong, Y. Tan, F. Krzakala, and S. Gigan, Large-scale optical reservoir computing for spatiotemporal chaotic systems prediction, *Physical Review X* **10**, 041037 (2020).
  - [12] J. Bongard and H. Lipson, Automated reverse engineering of nonlinear dynamical systems, *Proceedings of the National Academy of Sciences* **104**, 9943 (2007).
  - [13] M. Schmidt and H. Lipson, Distilling free-form natural laws from experimental data, *Science* **324**, 81 (2009).
  - [14] T. Wu and M. Tegmark, Toward an artificial intelligence physicist for unsupervised learning, *Physical Review E* **100**, 033311 (2019).
  - [15] H. Li, X.-q. Shi, M. Huang, X. Chen, M. Xiao, C. Liu, H. Chaté, and H. Zhang, Data-driven quantitative modeling of bacterial active nematics, *Proceedings of the National Academy of Sciences* **116**, 777 (2019).
  - [16] K. Champion, B. Lusch, J. N. Kutz, and S. L. Brunton, Data-driven discovery of coordinates and governing equations, *Proceedings of the National Academy of Sciences* **116**, 22445 (2019).
  - [17] R. Iten, T. Metger, H. Wilming, L. Del Rio, and R. Renner, Discovering physical concepts with neural networks, *Physical Review Letters* **124**, 010508 (2020).
  - [18] A. Decelle, V. Martin-Mayor, and B. Seoane, Learning a local symmetry with neural networks, *Physical Review E* **100**, 050102 (2019).
  - [19] Y.-i. Mototake, Interpretable conservation law estimation by deriving the symmetries of dynamics from trained deep neural networks, arXiv preprint arXiv:2001.00111

- (2019).
- [20] S. J. Wetzel, R. G. Melko, J. Scott, M. Panju, and V. Ganesh, Discovering symmetry invariants and conserved quantities by interpreting siamese neural networks, *Physical Review Research* **2**, 033499 (2020).
- [21] Z. Liu and M. Tegmark, Ai poincaré: Machine learning conservation laws from trajectories, arXiv preprint arXiv:2011.04698 (2020).
- [22] D. Misra, Mish: A self regularized non-monotonic activation function, arXiv preprint arXiv:1908.08681 (2019).
- [23] D. P. Kingma and J. Ba, Adam: A method for stochastic optimization, arXiv preprint arXiv:1412.6980 (2014).
- [24] A. Paszke, S. Gross, F. Massa, A. Lerer, J. Bradbury, G. Chanan, T. Killeen, Z. Lin, N. Gimelshein, L. Antiga, *et al.*, Pytorch: An imperative style, high-performance deep learning library, in *Advances in neural information processing systems* (2019) pp. 8026–8037.
- [25] Y. Takeuchi, *Global dynamical properties of Lotka-Volterra systems* (World Scientific, 1996).
- [26] H. Seungwoong and J. Hawoong, nokpil/conservnet, <http://doi.org/10.5281/zenodo.4491096> (2021), version: v1.0.0.